Journal of Alloys and Compounds 509 (2011) 61–65

Contents lists available at ScienceDirect

Journal of Alloys and Compounds

journal homepage: www.elsevier.com/locate/jallcom

Nanospherical and nanobundles of ZnO: Synthesis and characterization

Masoud Salavati-Niasari[a,b,*], Fatemeh Davar[a], Afsaneh Khansari[c]

[a] Institute of Nano Science and Nano Technology, University of Kashan, Kashan, P.O. Box 87317-51167, Iran
[b] Department of Inorganic Chemistry, Faculty of Chemistry, University of Kashan, Kashan, P.O. Box 87317-51167, Iran
[c] Department of Chemistry, Faculty of Science, University of Guilan, Rasht, P.O. Box 413354-1914, Iran

ARTICLE INFO

Article history:
Received 22 June 2010
Accepted 17 August 2010
Available online 26 August 2010

Keywords:
ZnO
Thermolysis
Thermal decomposition
Nanobundle
Nanospherical

ABSTRACT

ZnO nanospherical and nanobundles well dispersion have been synthesized using [(*N*,*N*′-bis(salicylaldehydo)ethylenediamine)zinc(II)]; [Zn(salen)] as precursor via two methods. Nanospherical of ZnO has been prepared via thermal decomposition of [Zn(salen)] in the presence of oleylamine at 290 °C for 90 min. Also nanobundle of ZnO has been synthesized via thermolysis of [Zn(salen)] in the air at 500 °C for 5 h. The as-synthesized products were characterized by powder X-ray diffraction (XRD), transmission electron microscopy (TEM), X-ray photoelectron spectroscopy (XPS) and scanning electronic microscopy (SEM). The room temperature photoluminescence (PL) spectra of both nanostructures are dominated by the green emission attributed to the oxygen vacancy (V_O) related donor–acceptor transition. Presence of several infrared (IR) inactive vibrational modes in the Fourier transform infrared (FT-IR) absorption spectra of the samples indicates a breakdown of translational symmetry in the nanostructures induced by native defects.

1. Introduction

Zinc oxide (ZnO), which has a bulk, direct band gap of 3.3 eV at room temperature with a free exciton binding energy of 60 meV, is among technologically important semiconducting materials with unique properties, such as optical transparency, electric conductivity, piezoelectricity and near-UV emission [1]. This metal oxide has a variety of applications, including chemical sensors [2], catalysts [3], UV light-emitters [4], photovoltaics [5] cantilevers [6] and other optoelectronic devices [7]. In addition, ZnO is nontoxic, at least in the bulk form, relatively cheap and stable in air [8].

In the past decade, various different physical or chemical synthetic approaches have been developed to produce ZnO, including vapor phase oxidation, thermal vapor transport and condensation (TVTC), chemical vapor deposition (CVD), precipitation, sol–gel, microemulsion, hydrothermal, solvothermal and sonochemical methods [9–21].

Currently, the method of thermal decomposition of organometallic precursors coordinating with solvents is being used more and more, which results in relatively stable nanoparticles for organic monolayer protection [22–26]. Choi et al. [27] reported a method for the large-scale synthesis of uniform-sized hexagonal shaped ZnO nanocrystals by thermolysis of Zn–oleate complex. Liu et al. [28] reported synthesis of ZnO nanoparticles from thermal decomposition of zinc acetylaceton; [$Zn(acac)_2$]; as a good precursor. Recently, our group [29] reported on the facile synthesis of ZnO nanoparticles via thermolysis of new precursor ([bis(2-hydroxyacetophenato)zinc(II)]) coordinating with solvents oleylamine and triphenylphosphine (TPP).

Another method for synthesizing metal oxides ultrafine powders, the metallorganic molecular precursor way, has been regarded as one of the most convenient and practical techniques, because it not only enables to avoid special instruments and complicated processes and severe preparation conditions, but also provides good control over purity, composition, homogeneity, phase and microstructure of the resultant products. By choosing a proper metallorganic molecular precursor, coupled with a rational calcining procedure [30–32] or other thermolysis processes, tiny and crystalline products could be obtained under the conditions significantly milder than those employed in conventional solid-state synthesis, usually in the absence of any other templates or surfactants [33].

In order for investigating on the role of precursor in size and shape of ZnO nanoparticles, in the continuation of previous works we decided to prepare ZnO nanocrystals from [(*N*,*N*′-bis(salicylaldehydo)ethylenediamine)zinc(II)]; [Zn(salen)] complex as a novel precursor. ZnO nanostructures with controlled morphology simply were synthesized through (i) thermal decomposition in the presence of oleylamine and (ii) simple calcinations of [(*N*,*N*′-bis(salicylaldehydo)ethylenediamine)zinc(II)]; [Zn(salen)] in the air. Through these techniques, nanospherical and nanobundles could be synthesized by a precise variation of the

* Corresponding author at: Institute of Nano Science and Nano Technology, University of Kashan, Kashan, P.O. Box 87317–51167, Iran. Tel.: +98 3621 5555333; fax: +98 361 5552935.
E-mail address: salavati@kashanu.ac.ir (M. Salavati-Niasari).

0925-8388/$ – see front matter © 2010 Elsevier B.V. All rights reserved.
doi:10.1016/j.jallcom.2010.08.060

method of synthesis. Here, we report a simple, green, low-cost, and reproducible process for the synthesis of ZnO nanocrystals. In this process, oleylamine was used as both the medium and the stabilizing reagent. To the best of our knowledge the use of [Zn(salen)] as precursor in nanoparticles synthesis approach is made for the first time. Optical properties of the obtained ZnO nanostructures were studied by room temperature photoluminescence and infrared spectroscopy techniques.

2. Experimental procedure

2.1. Materials

All the chemical reagents used in our experiments were of analytical grade and were used as received without further purification. Zinc(II) acetate dihydrate, salicylaldehyde and 1,2-ethylenediamine, oleyleamine, toluene and ethanol were obtained from Merck Co. and Aldrich Chemie and used as received.

2.2. Characterization

XRD patterns were recorded by a Rigaku D-max C III, X-ray diffractometer using Ni-filtered Cu Kα radiation. Elemental analyses were obtained from Carlo ERBA Model EA 1108 analyzer. Scanning electron microscopy (SEM) images were obtained using Philips XL-30ESEM equipped with an energy dispersive X-ray spectroscopy. Transmission electron microscopy (TEM) images were obtained utilizing Philips EM208 transmission electron microscope with an accelerating voltage of 100 kV. Fourier transform infrared (FT-IR) spectra were recorded with Shimadzu Varian 4300 spectrophotometer in KBr pellets. X-ray photoelectron spectroscopy (XPS) of the as-prepared products was performed on an ESCA-3000 electron spectrometer with nonmonochromatized Mg Kα X-ray as the excitation source. Thermogravimetric analysis (TGA) were carried out using a thermal gravimetric analysis instrument (Shimadzu TGA-50H) with a flow rate of 20.0 ml min^{-1} and a heating rate of 10 °C min^{-1}. Room temperature photoluminescence (PL) was studied on an F-4500 fluorescence spectrophotometer.

2.3. Preparation of N,N′-bis(salicylaldehyde)ethylenediamine; H_2salen [34]

The symmetrical Schiff base ligand *N,N′*-bis(salicylaldehyde)ethylenediimine, $C_{16}H_{16}N_2O_2$ (H_2salen), was prepared according to previously published methods, by refluxing 0.05 mol of salicylaldehyde (Merck-Schuchard, purified by distillation) and 0.025 mol of ethylenediamine (Aldrich Chemie, 99%, purified by distillation) in 30 ml of dried ethanol, for 30 min and cooling the reaction mixture. The Schiff base was separated as yellow needles and was recrystallized twice from methanol (yield 90%). The compound is stable at room temperature and has been characterized by IR spectroscopy and elemental analysis. The microanalytical results for the mass fractions *w* of C, H and N were as follows: for (H_2salen), $C_{16}H_{16}N_2O_2$, calculated C, 71.62; H, 6.01; N, 10.44, found C, 71.59; H, 6.03; N, 10.45%. The ligand was studied by d.s.c. over the temperature range 320–410 K and no phase transitions were found before the melting temperature (melting point: 168 °C). ^{1}HNMR ($CDCl_3$): δ 13.23 (br s, 2H, OH), 8.36 (s, 2H, H_e), 8.31 (m, 2H, H_b), 7.24 (dd, 2H, H_d), 6.96 (d, 2H, H_a), 6.86 (m, 2H, H_c), 3.95 (s, 4H, H_f, g).

2.4. Preparation of [N,N′-bis(salicylaldehydo)ethylenediamine]zinc(II); [Zn(salen)]

Ligand *N,N′*-bis(salicylaldehyde)ethylenediimine, (H_2salen), (2 mmol) was dissolved in 15 mL of ethanol, mixed with $Zn(OAc)_2.2H_2O$ (2 mmol, in ethanol) at 60 °C and stirred for 5 h. The yellow precipitates were washed several times using distilled water and dried in the air. The identification of the resulting products were based on powder X-ray diffraction (XRD), Fourier transform infrared spectrometer (FT-IR) and elemental analysis in addition to visual observation of the color of the reaction mixture. Anal. Calc. for [Zn(salen)]; $ZnC_{16}H_{14}N_2O_2$: C, 57.94; H, 4.25; N, 8.45%. Found: C, 57.98; H, 4.27; N, 8.48%.

2.5. Synthesis of ZnO nanospheres

The current synthetic procedure is a modified version of the method developed by Hyeon and co-workers for the synthesis of nanocrystals for metals that employs the thermal decomposition of transition metal complexes [35,36]. In this synthesis, ZnO nanospheres were prepared by the thermal decomposition of [Zn(salen)]–oleylamine complex as precursor. The [Zn(salen)]–oleylamine complex was prepared by the reaction of 0.7 g [Zn(salen)] with 6 ml of oleylamine. The resulting solution was heated to 170 °C and kept at that temperature for 90 min. Then, the temperature was increased to 240 °C and kept 70 min. As the reaction proceeded, the solution became slightly cloudy and dark gray, which demonstrated the formation of ZnO nanocrystals. The solution was then cooled to room temperature, and 10 ml ethanol was added to yield a white precipitate, which was then separated by centrifuging. The final products were washed with ethanol for at least three times to remove impurities, if any, and dried at 50 °C. The resulting product was easily redispersable in nonpolar solvent such as toluene (Scheme 1).

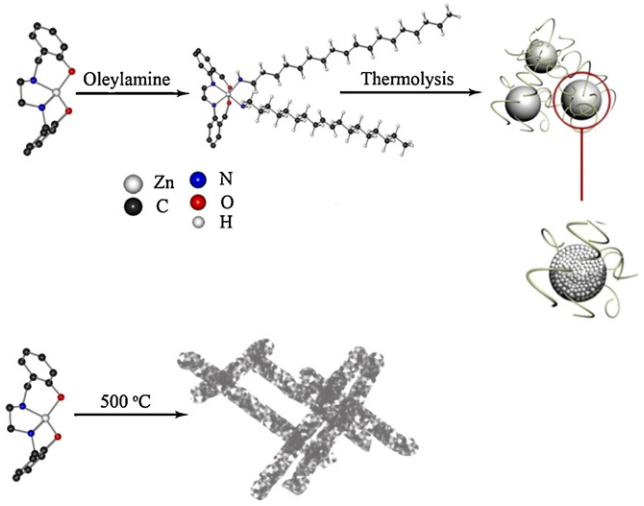

Scheme 1. Schematic for preparation of ZnO nanostructures.

2.6. Synthesis of ZnO nanobundle

ZnO nanobundles were produced by subjecting 0.01 mol of the as-prepared [Zn(salen)] powders to thermal treatment at a relatively low temperature (500 °C) in the air. An average temperature increase of 30 °C is recorded every minute, before the temperature reached 500 °C, and after keeping the thermal treatment at 500 °C for 5 h, it was allowed to cool unaffectedly in the room temperature. The ZnO nanobundle was washed with ethanol and distilled water for three times and dried in the air at 50 °C.

3. Results and discussion

Fig. 1 shows the XRD patterns ($10° < 2\theta < 80°$) of the obtained [Zn(salen)] precursor (Fig. 1a), ZnO nanospherical (Fig. 1b) and ZnO nanobundles (Fig. 1c). The XRD pattern in Fig. 1b is consistent with the spectrum of ZnO, and no peak attributable to possible

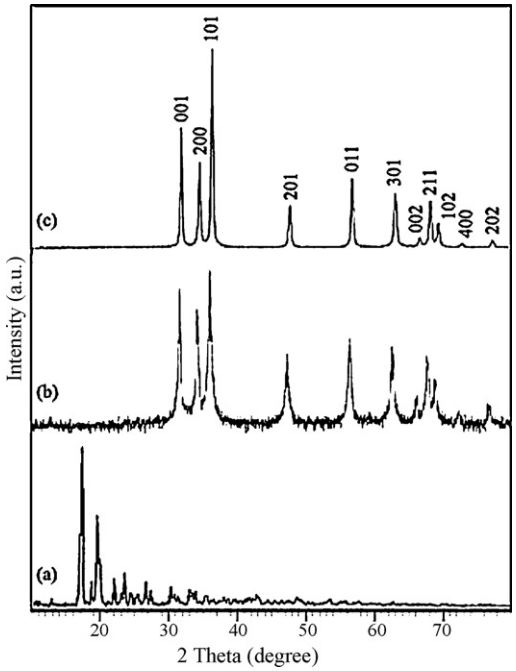

Fig. 1. XRD patterns of (a) [Zn(salen)], (b) ZnO nanosphericals and (c) ZnO nanobundles.

impurities is observed. All of the reflection peaks of the XRD pattern for ZnO nanospherical that can be indexed well to hexagonal phase ZnO (space group: *P*63*mc*; JCPDS No. 79-0205), with calculated cell parameters $a = 3.25$ Å and $c = 5.21$ Å. Fig. 1c shows the XRD pattern of ZnO nanobundles can be indexed well to hexagonal phase ZnO (JCPDS No. 79-0205) with calculated cell parameter. The sharp diffraction peaks manifestation shows that the obtained ZnO nanostructures have high crystallinity. The crystallite sizes of the as-synthesized ZnO, D_c, were calculated from the major diffraction peaks of the base of (1 0 1) using the Scherrer formula (Eq. (1)):

$$D_c = \frac{K\lambda}{\beta \cos\theta} \quad (1)$$

where K is a constant (ca. 0.9), λ is the X-ray wavelength used in XRD (1.5418 Å), θ is the Bragg angle and β is the pure diffraction broadening of a peak at half-height, that is broad due to the crystallite dimensions. The size of the crystallite was estimated from Debye–Scherrer equation 21 nm.

Fig. 2 shows a comparison of FT-IR spectrum of (a) [Zn(salen)], (b) ZnO nanospherical, (c) free oleylamine and (d) ZnO nanobundles. The spectra of the [Zn(salen)] gave evidences for the synthesis of the complex since two bands at 1550 cm^{-1} (attributed to νC=C) and at 1600 cm^{-1} (attributed to νC=N) which are characteristic of the [Zn(salen)] complex appeared the IR spectra of the precursor. The broad absorption bands at ~3400 cm^{-1} encompass the O–H stretching vibrations of adsorbed water [37]. The strong peak around 475 cm^{-1} shows a distinct stretching mode of crystal ZnO. Presence of oleylamine group on ZnO nanoparticles (Fig. 2b) is indicated by two peaks at 2945 and 2853 cm^{-1} which represents the C–H stretching modes of the oleylamine carbon chain and matches with oleylamine spectrum (Fig. 2c). In our measurement, number of weak peaks between ν1000 and 1400 cm^{-1} are attributable to the asymmetric stretching of the $-CH_2$ groups, terminal $-CH_3$ and =CH of oleylamine. The broad absorption band of O–H stretching (~3400 cm^{-1}) is due to adsorbed water on the external surface of the samples during handling to record the spec-

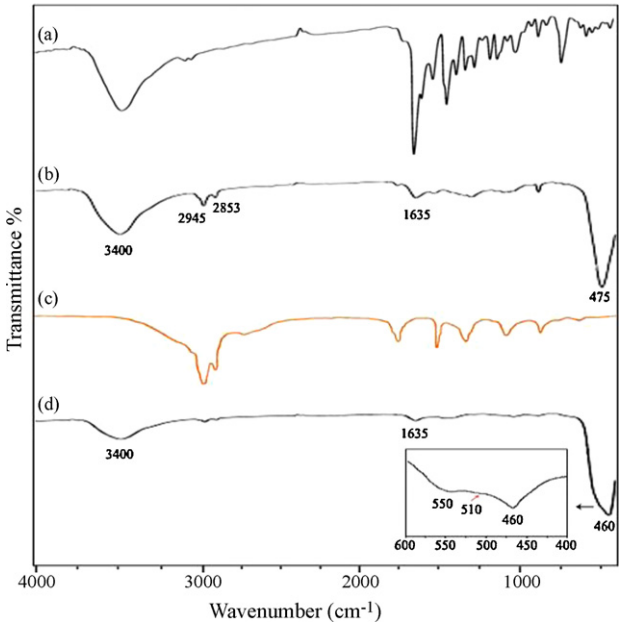

Fig. 2. FT-IR spectra of (a) [Zn(salen)], (b) ZnO nanospherical, (c) free oleylamine and (d) ZnO nanobundles.

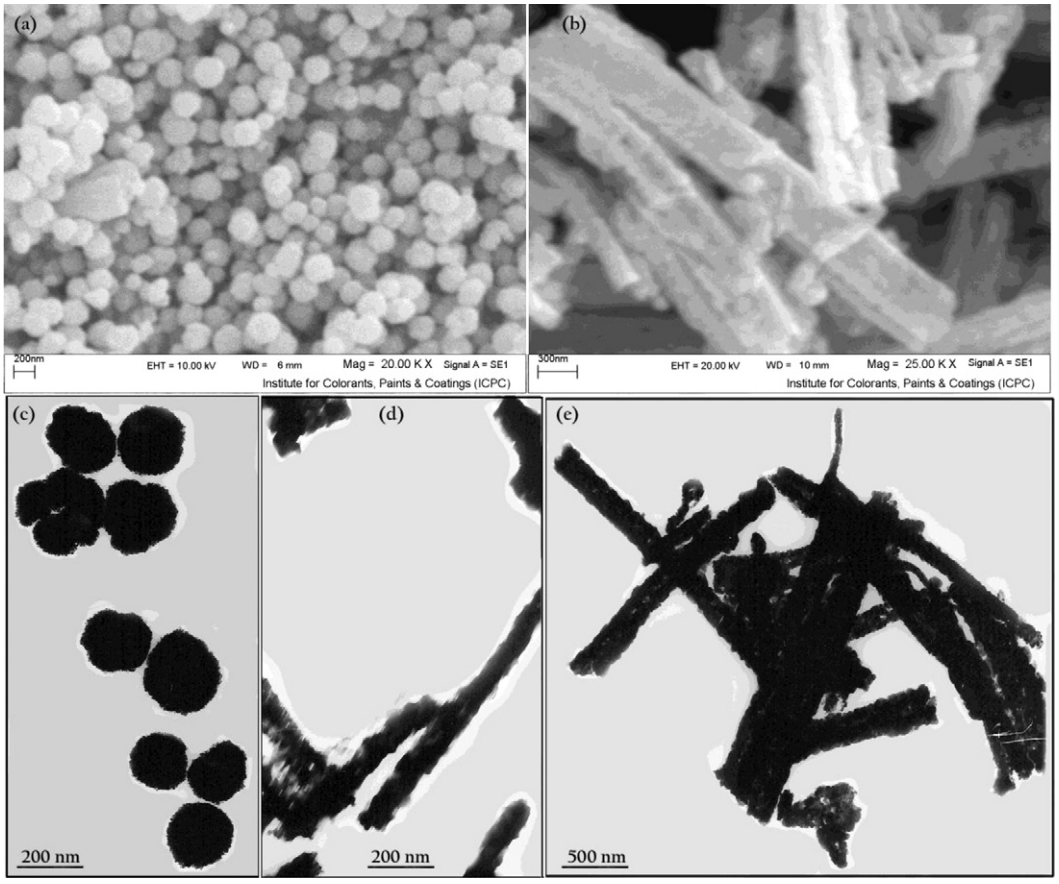

Fig. 3. SEM images of (a) ZnO nanospherical and (b) ZnO nanobundles. TEM images of (c) ZnO nanospherical and (d and e) ZnO nanobundles.

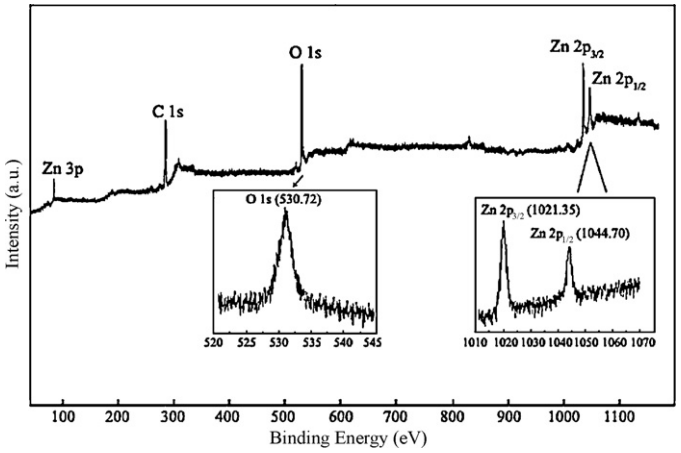

Fig. 4. The wide XPS spectrum of the ZnO nanocrystals. (Inset shows the high-resolution XPS spectra taken for the Zn 2p and O 1s region of ZnO).

tra. The H–OH bending vibration appears at 1635 cm^{-1} [38]. The strong broad peak around 460 cm^{-1} shows a distinct stretching mode of crystal ZnO in Fig. 2d. There was no evidence of free precursor [Zn(salen)] in the as-prepared sample, if there was absorption of [Zn(salen)] on the surface of the ZnO particles, a distinct carbonyl peak around 1600 cm^{-1} and the peaks attributed to aromatic rings around 600–1000 cm^{-1} (Fig. 2a) should appear in the FT-IR spectrum. The inset of Fig. 2 shows the FT-IR spectra of the ZnO nanobundles in the frequency range where vibrational modes related to ZnO are observed. For as-prepared ZnO nanobundles, three bands located at about 550, 510 and 460 cm^{-1} are observed. These bands do not match with any IR-active vibrational mode for bulk ZnO [39]. Several authors have reported similar anomalous vibrational modes in ZnO attributed to local vibrational modes of impurities or defects [39].

The microstructures and morphology of the products have been examined by SEM and TEM images (Fig. 3a–e), respectively. Fig. 3a and c shows spherical shape of the obtained product by thermal decomposition [Zn(salen)] in the presence of oleylamine. Fig. 3a gives an overall view of the product, revealing the surface morphology of the ZnO spheres by SEM image. It can be seen that the products are tiny, aggregated nanoparticles with spherical shapes. TEM image of the product has been given in Fig. 3b. Fig. 3b shows ZnO microspheres that have been formed of small spheres formed of ZnO nanoparticles. The size of nanoparticles obtained from the XRD diffraction patterns are in close agreement with the TEM studies which shows average size of 10 nm. These sizes are nearly spherical and confirm the SEM micrograph. It is observed that in spite of agglomeration of nanospheres, they have a narrow size distribution. Fig. 3(c)–(e) shows SEM and TEM images of ZnO nanobundles. As shown in Fig. 3d and e nanobundles with a diameter of ca. 20 nm have been observed. These nanobundles have likely been formed by the aggregation of ZnO nanospheres drawn together. Further observation at higher magnification reveals that each nanobundles actually consists of nanoparticles that are individually ca. 20 nm in diameter (Fig. 3e). These nanoparticles are sequentially connected together to form nanobundles with lengths on the order of ca. 1–2 μm.

Further evidence for the purity and composition of the products was obtained by X-ray photoelectron spectra (XPS). The survey XPS spectra of the samples suggested the presence of Zn and O, as well as C reference. The binding energies obtained in the XPS analysis were corrected for specimen charging by referencing the C 1s to 284.60 eV. The high-resolution spectrum of Zn 2p is given in Fig. 4. The obtained binding energy (BE) values of Zn $2p_{3/2}$ and $2p_{1/2}$ are 1021.53 and 1044.70 eV, respectively. The spin–orbit splitting is

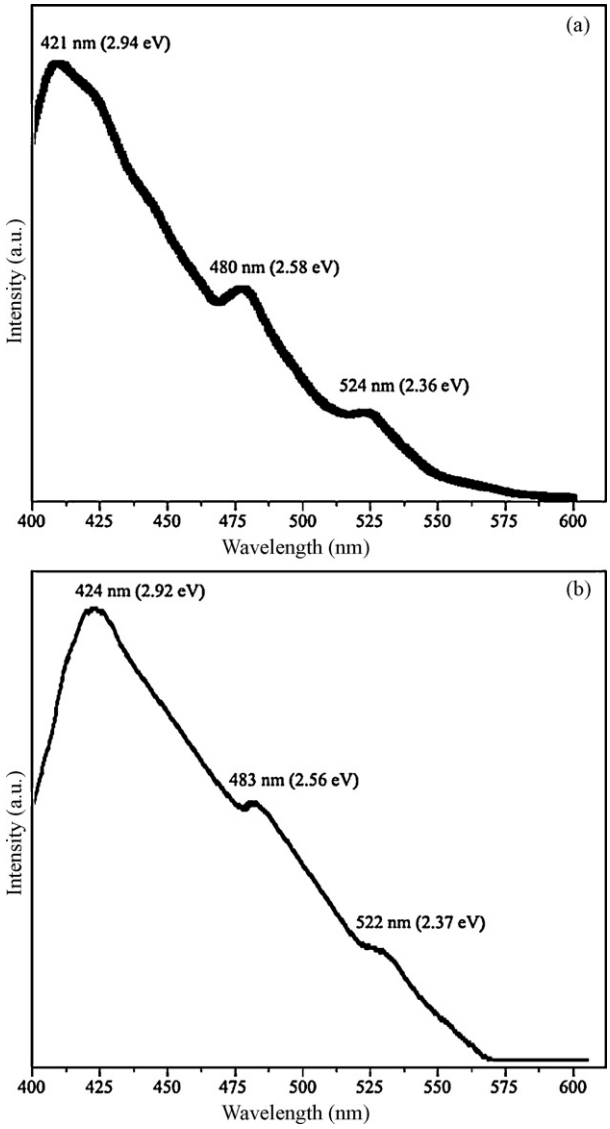

Fig. 5. Room temperature PL spectra for (a) ZnO nanospherical and (b) ZnO nanobundles.

the difference between BE values of Zn $2p_{3/2}$ and Zn $2p_{1/2}$ levels. The observed spin–orbit splitting is 23.17 eV, just the same as zinc oxides [40]. The oxygen spectrum has also been shown in Fig. 4. The peak O 1s at 530.72 eV can be attributed to oxygen O^{2-} in the lattice of zinc oxide. This indicates the formation of ZnO as a pure product of the decomposition of [Zn(salen)] as single precursor. No obvious peaks for other elements or impurities were observed.

Room temperature PL spectra of the zinc oxide nanostructures are shown in Fig. 5 (excitation = 300 nm). The spectrum of the ZnO nanospheres (Fig. 5a) mainly consists of three emission bands: (i) a strong UV emission band at 421 nm (2.94 eV), (ii) a week blue-green band at 480 nm (2.58 eV) and (iii) a green band at 524 nm (2.36 eV). The strong UV emission corresponds to the exciton recombination related near-band edge emission of ZnO [41,42]. Wang and co-workers calculated the energy levels of the intrinsic defects in undoped ZnO films and indicated them as – oxygen vacancy (V_O), zinc vacancy (V_{Zn}), interstitial oxygen (O_i), interstitial zinc (Zn_i) and antisite oxygen (O_{zn}) [43]. The weak blue-green emission corresponds to the singly ionized oxygen vacancy in ZnO, and this emission results from the recombination of a photo-generated hole with the individually ionized charge state of the specific defect [44,45] as in the case of ZnO nanowires reported by Wang and

Gao [46]. The low intensity of the green emission may be due to the low density of oxygen vacancies during the preparation of the ZnO, whereas the strong room temperature UV emission intensity should be attributed to the high purity with perfect crystallinity of the synthesized ZnO. The PL spectrum for ZnO nanobundles are given in Fig. 5b. In this picture three peaks were observed, but in comparison to Fig. 5a, a little red shift can be observed, because of size effect.

4. Conclusion

In conclusion, ZnO nanospheres were synthesized by thermolysis of [Zn(salen)] as precursor using oleylamine and without it under mild conditions. The crystallite size of the nanocrystals can be estimated between 20 and 30 nm. Since the hired precursor is cheap, air-stable, and readily available for many metal elements, this synthesis may represent a rather environmentally friendly and general approach towards many other metal oxide nanocrystals. This precursor has steric hindrance and therefore there was no need to use two surfactants for size control. Also the novel precursor was thermally treated without using any surfactant and ZnO nanobundles were synthesized. Moreover thermal decomposition method employs an inexpensive, reproducible process for the large-scale synthesis of ZnO nanocrystals.

Acknowledgement

Authors are grateful to council of University of Kashan for providing financial support to undertake this work.

References

[1] T. Kawano, H. Imai, Cryst. Growth Des. 6 (2006) 1054–1056.
[2] J. Tamaki, Sens. Lett. 3 (2005) 89–98.
[3] M. Kurtz, J. Strunk, O. Hinrichsen, M. Muhler, K. Fink, B. Meyer, C. Wöll, Angew. Chem. Int. Ed. 44 (2005) 2790–2794.
[4] C.L. Yang, J.N. Wang, W.K. Ge, L. Guo, S.H. Yang, D.Z. Shen, J. Appl. Phys. 90 (2001) 4489–4493.
[5] M. Izaki, K.-T. Mizuno, T. Shinagawa, M. Inaba, A. Tasaka, J. Electrochem. Soc. 153 (2006) C668–C672.
[6] S.H. Lee, S.S. Lee, J.-J. Choi, J.U. Jeon, K. Ro, Microsyst. Technol. 11 (2005) 416–423.
[7] L. Vayssieres, K. Keis, S.-E. Lindquist, A. Hagfeldt, J. Phys. Chem. B 105 (2001) 3350–3352.
[8] K.J. Hartlieb, C.L. Raston, M. Saunders, Chem. Mater. 19 (2007) 5453–5459.
[9] J.Q. Hu, Q. Li, N.B. Wong, C.S. Lee, S.T. Lee, Chem. Mater. 14 (2002) 1216–1219.
[10] J.Y. Lao, J.Y. Huang, D.Z. Wang, Z.F. Ren, Nano Lett. 3 (2003) 235–238.
[11] J.Y. Lao, J.G. Wen, Z.F. Ren, Nano Lett. 2 (2002) 1287–1291.
[12] P.V. Radovanovic, N.S. Norberg, K.E. McNally, D.R. Gamelin, J. Am. Chem. Soc. 124 (2002) 15192–15193.
[13] E.W. Seelig, B. Tang, A. Yamilov, H. Cao, R.P.H. Chang, Mater. Chem. Phys. 20 (2003) 257–263.
[14] L. Guo, Y.L. Ji, H. Xu, P. Simon, Z. Wu, J. Am. Chem. Soc. 124 (2002) 14864–14865.
[15] B. Cheng, E.T. Samulski, Chem. Commun. 8 (2004) 986–987.
[16] Z. Jia, L. Yue, Y. Zheng, Z. Xu, Mater. Chem. Phys. 107 (2008) 137–141.
[17] J. Joo, S.G. Kwon, J.H. Yu, T. Hyeon, Adv. Mater. 17 (2005) 1873–1877.
[18] N. Bouropoulos, I. Tsiaoussis, P. Poulopoulos, P. Roditis, S. Baskoutas, Mater. Lett. 62 (2009) 3533–3535.
[19] V.G. Kessler, J. Sol–Gel Sci. Technol. 51 (2009) 264–271.
[20] F. Mohandes, F. Davar, M. Salavati-Niasari, J. Magn. Magn. Mater. 322 (2010) 872–877.
[21] X. Liu, B. Geng, Q. Du, J. Ma, X. Liu, Mater. Sci. Eng. A 448 (2007) 7–14.
[22] M. Salavati-Niasari, N. Mir, F. Davar, J. Alloys Compd. 493 (2010) 163–168.
[23] F. Davar, Z. Fereshteh, M. Salavati-Niasari, J. Alloys Compd. 476 (2009) 797–801.
[24] M. Salavati-Niasari, N. Mir, F. Davar, Appl. Surf. Sci. 256 (2010) 4003–4008.
[25] M. Salavati-Niasari, F. Davar, Z. Fereshteh, J. Alloys Compd. 494 (2010) 410–414.
[26] F. Davar, M. Salavati-Niasari, Z. Fereshteh, J. Alloys Compd. 496 (2010) 638–643.
[27] S.-H. Choi, E.-G. Kim, J. Park, K. An, N. Lee, S.C. Kim, T. Hyeon, J. Phys. Chem. B 109 (2005) 14792–14794.
[28] J.F. Liu, Y.Y. Bei, H.P. Wu, D. Shen, J.Z. Gong, X.G. Li, Y.W. Wang, N.P. Jiang, J.Z. Jiang, Mater. Lett. 61 (2007) 2837–2840.
[29] M. Salavati-Niasari, F. Davar, Z. Fereshteh, Chem. Eng. J. 146 (2009) 498–502.
[30] X. Nie, Q. Zhao, H. Zheng, J. Cryst. Growth 289 (2006) 299–302.
[31] D. Bayot, M. Degand, M. Devillers, J. Solid State Chem. 178 (2005) 2635–2642.
[32] T. Ould-Ely, J.H. Thurston, K.H. Whitmire, C. R. Chim. 8 (2005) 1906–1921.
[33] Y.C. Zhang, J.Y. Tang, G.L. Wang, M. Zhang, X.Y. Hu, Cryst. Growth 294 (2006) 278–282.
[34] G. Li, L. Chen, J. Bao, T. Li, F. Mei, Appl. Catal. A: Gen. 346 (2008) 134–139.
[35] J. Park, E. Kang, S.U. Son, H.M. Park, M.K. Lee, J. Kim, K.W. Kim, H. Noh, J. Park, C.J. Bae, J. Park, T. Hyeon, Adv. Mater. 17 (2005) 429–434.
[36] M. Salavati-Niasari, F. Davar, Mater. Lett. 63 (2009) 441–443.
[37] K. Nakamoto, Infrared Spectra of Inorganic and Coordination Compound, 4th ed., Chemical Industry Press, Beijing, 1991.
[38] M. Salavati-Niasari, N. Mir, F. Davar, J. Alloys Compd. 476 (2009) 908–912.
[39] G. Muñoz-Hernández, A. Escobedo-Morales, U. Pal, Cryst. Growth Des. 9 (2009) 297–302.
[40] F.J. Manjón, B. Marí, J. Serrano, A.H. Romero, J. Appl. Phys. 97 (2005) 053516–053519.
[41] S.C. Lyu, Y. Zhang, H. Ruh, H. Lee, H. Shim, E. Suh, C.J. Lee, Chem. Phys. Lett. 363 (2002) 134–138.
[42] L. Bergman, X.B. Chen, J.L. Morrison, J. Huso, A.P. Purdy, J. Appl. Phys. 96 (2004) 675–683.
[43] Z. Fang, Y. Wang, D. Xu, Y. Tan, X. Liu, Opt. Mater. 26 (2004) 239–242.
[44] S. Monticone, R. Tufeu, A.V. Kanaev, J. Phys. Chem. B 102 (1998) 2854–2862.
[45] B.D. Yao, Y.F. Chan, N. Wang, Appl. Phys. Lett. 81 (2002) 757–759.
[46] J. Wang, L. Gao, Solid State Commun. 132 (2004) 269–271.